

Crumpling of a stiff tethered membrane

J.A. Åström¹, J. Timonen², and Mikko Karttunen³

¹*Centre for Scientific Computing, P.O. Box 405, FIN-02101 Esbo, Finland*

²*Department of Physics, University of Jyväskylä, P.O. Box 35, FIN-40014 University of Jyväskylä, Finland and*

³*Biophysics and Statistical Mechanics Group, Laboratory of Computational Engineering, Helsinki University of Technology, P.O. Box 9203, FIN-02015 HUT, Finland*

(Dated: September 5, 2021)

A first-principles numerical simulation model for crumpling of a stiff tethered membrane is introduced. In our model membranes, wrinkles, ridge formation, ridge collapse, as well as the initiation of stiffness divergence, are observed. The ratio of the amplitude and wave length of the wrinkles, and the scaling exponent of the stiffness divergence, are consistent with both theory and experiment. We observe that close to the stiffness divergence there appears a crossover beyond which the elastic behavior of a tethered membrane becomes similar to that of dry granular media. This suggests that ridge formation in membranes and force-chain network formation in granular packings are different manifestations of a single phenomenon.

PACS numbers: 46.25.-y, 68.60.Bs, 05.70.Np, 82.20.Wt

Crumpling of, e.g., sheets of paper, is an everyday phenomenon that one easily passes without much extra attention. For physicists, however, crumpling has for a long time been a topic of intense research. In addition to fundamental statistical mechanic properties [1], issues such as scaling of strength and energy [2, 3], geometry and singularities [4, 5], and even acoustic emission [6] and crumpling related phenomena in soft matter systems [7], have become topics of increasing interest. In this article, we present a first-principles numerical simulation model for crumpling of a stiff tethered membrane, and relate the problem to formation of force chain networks in granular media [8, 9].

Crumpling of a thin elastic sheet or a stiff membrane demands deformation energy. At very small strains a membrane is uniformly compressed. Thin structures are, however, sensitive to buckling. At first buckling appears as wrinkles. The wave length and the amplitude of the wrinkles depend on the conditions of the external loading and on the dimensions of the membrane [10]. As crumpling proceeds the deformation energy begins to concentrate in narrow ridges and conical peaks [2, 4]. Upon crumpling of a piece of paper, for example, the strain at the ridges and peaks become so large that irreversible plastic yielding takes place. After the paper is stretched out again, the ridge pattern can clearly be observed.

Another characteristic feature of membrane crumpling is that the effective stiffness of a crumpled membrane increases fast when the degree of crumpling becomes large. The ultimate limit of crumpling would be to press a membrane into a more or less cubic form with a volume corresponding to that of the volume of the membrane itself. In practice this limit can hardly be reached. Squeezing a piece of paper as hard as possible between the hands, results in a ball that typically contains about 75% air [11]. The behavior of the effective stiffness has been investigated by carefully monitored experiments, and for a crumpled membrane it displays a power-law divergence as the dense packing limit is approached [11]. The suggested explanation to the power-law divergence is that the total ridge length diverges in a scale invariant way as the

porosity inside the crumpled membrane vanishes.

In order to study wrinkles, ridge formation, and the effective stiffness in crumpled membranes, we constructed a numerical model for stiff tethered membranes. The tethered membrane consists of frictionless spheres with stiffness Y_s arranged in a triangular lattice. Each sphere has a mass m and moment of inertia I , and is connected to its neighbors by massless elastic beams which have both bending and tensile stiffness. It is reasonable to use a higher Young's modulus for the spheres (Y_s) than for the beams (Y_b). In the simulations here we chose $Y_s = 10^7$ and $Y_b = 5 \times 10^3$. The membrane is placed horizontally (i.e., in the xy plane) in the middle of a rigid cube of size $X^3(t)$, where X is time dependent. Small random fluctuations of the z component of the centers of mass of the spheres are introduced to avoid perfect symmetry. Newtonian dynamics is applied.

The environment inside the box is set to be strongly dissipative (the membrane can be thought of being immersed in a highly viscous fluid). This means that a force proportional to velocity, $(d\vec{x})$, slows down the motion of each sphere. The membrane dimensions are considered to be large enough for temperature fluctuations to be negligible (e.g. a paper sheet). For computational reasons the membrane cannot contain more than about 10^5 degrees of freedom, which sets a limit on its size. Wrinkles and the onset of ridge formation is nevertheless observed. Also the beginning of a power-law divergence of the effective stiffness with an exponent close to the one observed experimentally is seen. However, as porosity reaches a low enough value, the effective stiffness begins to deviate from the experimental power law. At low porosities the effective stiffness of a tethered membranes behaves in the same way as that of a packing of solid spheres [12].

Figure 1 shows a snapshot from a simulation displaying a few wrinkles at $t = 200$. By minimizing the elastic energy it can be demonstrated that the relation between the wave-length (λ) and the amplitude (A) of the wrinkles is generally given by $A/\lambda \sim (\Delta/W)^{1/2}$, where W is the width and Δ the compression of the membrane perpendicular to the wrinkles [10].

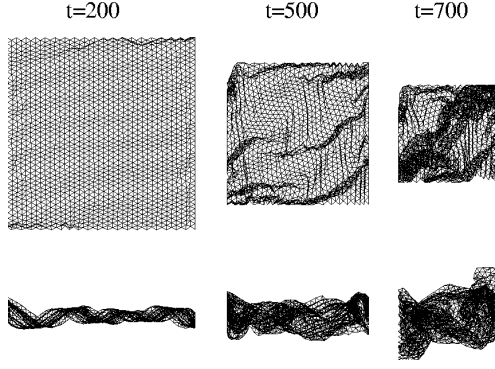


FIG. 1: Snapshots of a crumpling membrane. Top views (above) and side views (below) at times $t = 200, 500, 700$ are displayed. At $t = 200$ wrinkles can be observed. At $t = 500$ ridges have formed and begun to collapse. At $t = 700$ the membrane is at the beginning of the stiffness scaling regime, $(X - X_c)/X_c \approx 1.6$.

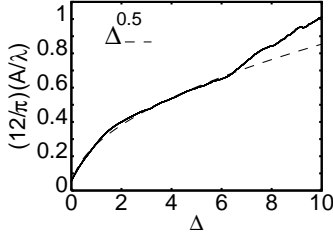


FIG. 2: The ratio of wrinkle amplitude and wave-length (A/λ) as a function of membrane compression Δ . The simulation result is compared to the theoretical prediction $A/\lambda \propto \sqrt{\Delta}$.

This relation is tested in Fig. 2 for the model membranes. The square-root relation between A/λ and Δ holds up to $\Delta \approx 6$ (here $W \approx 23.4$).

Deformation of ridges in controlled geometries has been thoroughly investigated both numerically and theoretically [2, 3, 5, 13, 14, 15, 16, 17]. The elastic deformation energy of a ridge of length L scales as $\kappa(L/\delta)^{1/3}$, where δ is the thickness of the sheet and κ its bending modulus. By taking advantage of this result, and following the derivation in Ref. [11], the scaling of stiffness of a membrane can be estimated: A crumpled sheet is divided into facets by the ridges. Ridges surrounding a facet of size L^2 have a length proportional to L . Such facets should fill a space of size L^3 . This leads to a bulk stiffness divergence of the form $K = -VdP/dV \propto V^{-11/3}$, when the volume V surrounding the sheet decreases under the influence of pressure P . This is not quite consistent with experimental findings. In Ref. [11] K was reported to scale as $K \propto (V_c - V)^{-\alpha}$ with $\alpha \approx 2.85$. Notice that this scaling relation can also be expressed in the forms $F \propto (\phi_c - \phi)^{-\alpha+1}$ and $F \propto (X - X_c)^{-\alpha+1}$, where F is the external force applied on the membrane, ϕ the solid volume fraction, and $X(t)$ the time dependent linear dimension of the crumpling membrane.

To investigate possible ridge formation in the simulations, we compare the local bending to the local energy. We define the sum of the dot products of nearest neighbor bonds along

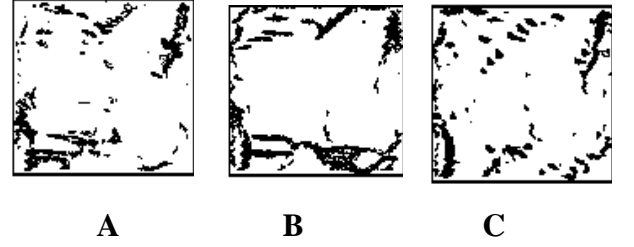


FIG. 3: Contour maps (at $t = 400$) of the spatial locations of (A) the highest local bendings $p(\vec{x}, t) < 0.6$, (B) the highest elastic energy of the beams $E_b(\vec{x}, t)$, and (C) the highest contact elastic energies of the spheres $E_s(\vec{x}, t)$.

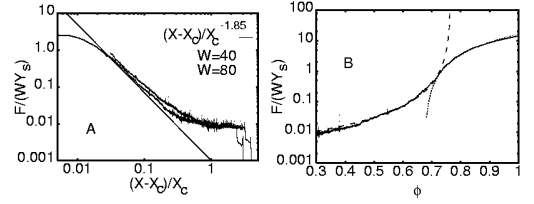


FIG. 4: (A) The total force F on the box surrounding a membrane scaled by sphere Young's modulus Y_s and linear membrane length W as function of $(X - X_c)/X_c$. Data is shown for membranes of linear size $W = 40, 80$. The solid line shows the experimentally observed [11] power-law divergence $F(X) \sim (X - X_c)^{-1.85}$. (B) $F/(WY_s)$ as function of solid volume fraction ϕ . The scaling of membrane stiffness $(\phi_c - \phi)^{-1.85}$, with $\phi_c \approx 0.76$, and the scaling of granular stiffness $(\phi - \phi_c)^{1.62}$, with $\phi_c \approx 0.67$ are compared to the simulation results.

the three principal directions in a triangular lattice as a measure of the local bending of the membrane,

$$p(\vec{x}, t) = \frac{1}{3} \sum_{i=1}^3 \frac{\vec{l}_i^n(t) \cdot \vec{l}_i^m(t)}{l_i^n l_i^m}. \quad (1)$$

This is then compared to the local elastic energies of the beams

$$E_b(\vec{x}, t) = \sum_{i=1}^6 \int_0^t \mathbf{F}(Y_b, \vec{x}(t)) d\vec{x}(t). \quad (2)$$

In Eq. (1), l^m and l^n are the lengths of the beams on the opposite sides of a lattice site. In Eq. (2), the elastic force $\mathbf{F}(Y_b, \vec{x}(t))$ is integrated over the corresponding displacement and summed over the six degrees of freedom for each site.

In addition, the elastic deformation energy of spheres in contact can be used to identify ridges. It can be written as

$$E_s(\vec{x}, t) = \sum_{i=1}^n \frac{1}{2} Y_s \delta_s^2, \quad (3)$$

where Y_s is the stiffness of the spheres and δ_s the virtual 'overlap' of spheres in contact. The sum is taken over all contacts.

Figure 3 shows contour plots of the lowest values of $p(\vec{x}, t)$ and the highest values of $E_b(\vec{x}, t)$ and $E_s(\vec{x}, t)$ at an early

stage of the crumpling process ($t = 400$). It is quite obvious that E_b and E_s reach their highest values at the locations of high local bending. The patterns are quite complex, but elongated structures, i.e. ridges, can be seen in the figure. As crumpling proceeds, ridges grow and collapse and the membrane folds. For later crumpling stages it is no longer possible to visibly detect ridges as the patterns become too complex.

The effective bulk stiffness of a membrane can be monitored, e.g., through its stress-strain curve. This is simply the total force F on the walls of the box surrounding the membrane, divided by the linear size W of the membrane (F/W) as a function of $X(t)$. Initially $F(t)/W$ increases fairly linearly until the membrane begins to buckle and fold. As the dense packing limit is approached, F/W begins to increase rapidly. Finally, when the membrane almost fills the box, a saturation regime is entered.

It is important to notice that there are three types of dense packing limits: 1) The tightest packing is achieved when the membrane volume is equal to the volume of its container. In this limit, the solid volume fraction is $\phi_1 = 1.0$. 2) Hard-core spheres. Here, the tightest packing is an FCC lattice with $\phi_2 = \pi\sqrt{2}/6 \approx 0.74$. 3) A random dense packing of spheres with $\phi_3 \approx 0.63$. For membranes it seems that the stiffness divergence takes place at $\phi_c \approx 0.75$ which is close to ϕ_2 . The regime of saturating stiffness is, however, entered well before this limit is reached.

Figure 4A shows $F/(Y_s W)$ for membranes with 10^4 and 4×10^4 degrees of freedom (each simulation demands about $10^6 - 10^7$ time steps). The simulation results are compared to the experimental result reported by Matan *et al.* [11], who found that $F(X) \propto (X - X_c)^{-\alpha+1}$, with $\alpha \approx 2.85$. Figure 4A shows good agreement between simulations and experiment until saturation sets in at $(X - X_c)/X_c \approx 0.03$.

At saturation there is a crossover to a different type of stiffness behavior. Beyond saturation the beams no longer affect the stiffness of the membranes. Instead, the membranes begin to behave like granular packings [12]. The stiffness of a 3D packing of solid spherical grains scales like $(\phi - \phi_c)^\beta$, with $\beta \approx 1.62$, and the critical volume is $\phi_c \approx 0.6 - 0.7$ depending on the form of interaction between the grains. Figure 4B shows a comparison between simulations and the scaling behavior of $F(\phi)$ in the two mentioned regimes.

By following the energy contents in a membrane from the initially flat membrane to a fully crumpled state, it is possible to determine the energy component responsible for the stiffness divergence seen in Fig. 4. The external energy $\int_t F(t) [X(t) - X(0)] dt$ is compared to the internal energy of the membrane in Fig. 5A. There is no difference between the external and internal energies as energy conservation also demands.

The internal energy can be split into five terms that are related to the force terms in the general equation of motion

$$m\ddot{x} + d\dot{x} + \mathbf{K}\vec{x} + Y_s\vec{\delta}_s = \vec{f}_{ext}. \quad (4)$$

Here, x is the displacement, m the mass, d the damping coefficient, \mathbf{K} the stiffness matrix, $\vec{\delta}_s$ the deformations (or vir-

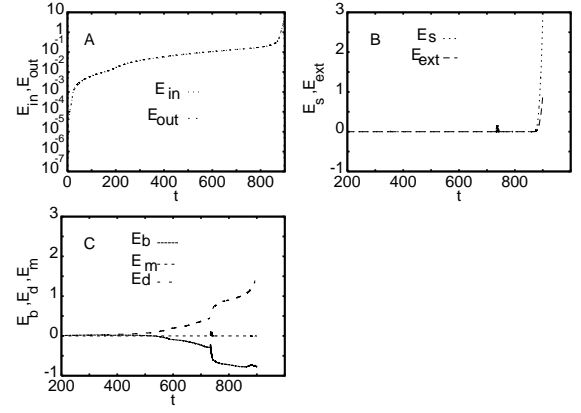


FIG. 5: (A) Internal and external energies as functions of time t . (B) E_s and E_{ext} as functions of t . (C) E_d , E_b and E_m as functions of t .

tual overlap) of spheres in contact, and \vec{f}_{ext} are forces applied on the walls of the box surrounding the membrane. The related energy terms are the following: (1) The elastic energy of the beams, E_b . (2) The compression energy at the contacts between spheres, E_s . (3) The compression energy of the spheres against the external walls, $E_{ext} = 0.5 \sum Y_w \delta_w^2$. (4) The energy dissipated through damping, $E_d = \int_t \vec{F}_d d\vec{x}$. (5) The kinetic energy of the spheres, $E_m = 0.5 \sum m \dot{\vec{x}}^2$. These energy components are shown separately as functions of time in Figs. 5B and 5C. The diverging terms are E_s and E_{ext} . The divergence of E_{ext} is rather trivial as it is just the deformation energy of the box surrounding the membrane. It is thus the energy E_s that causes the stiffness divergence. This explains to some extent why there is a crossover to the stiffness behavior of granular packings. When the deformation energy at the contacts between spheres dominate over other energy terms, the beams no longer play a role in the membrane stiffness.

Since there are two different scaling behaviors of stiffness, and both regimes are dominated by E_s , one would expect that at the crossover point there appears a qualitative change in the function describing the distribution of contact energies of the spheres. There is, however, no indication of such a qualitative change as is demonstrated in Fig. 6, which means that, at the crossover, ridges are simultaneously force chains. When comparing the topology of the network of ridges in crumpled membranes and that of the force-chain network in dry granular materials [8, 9], one notices that both are essentially one-dimensional lines of localized deformation energy, and form complicated networks in three-dimensional space. Based on these observations, it is plausible to draw the conclusion that the ridge formation and force-chain formation are not separate phenomena, but different manifestations of a single phenomenon. The crossover between the two then only marks the region where the membrane thickness begins to limit the density of network lines.

In conclusion, we have demonstrated for the first time that

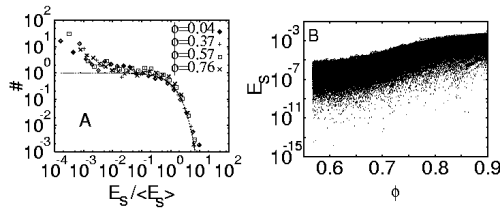


FIG. 6: (A) Distribution functions for the deformation energies at contacts between spheres for different solid volume fractions $\phi = 0.04, 0.37, 0.57, 0.76$. The distribution functions are compared to the equilibrium distribution $\exp(-E_s)$ [18]. (A) E_s as a function of ϕ . The crossover that takes place at $\phi \approx 0.72$ is not visible in the data.

a numerical model of a tethered membrane can reproduce the theoretically predicted wrinkling and ridge formation, and experimentally observed stiffness divergence. The early-stage ridges can be traced both by the elastic deformations of the beams and by the contact deformations of spheres in a tethered membrane. The divergence of the effective stiffness is a result of the divergence of the contact energy of the spheres. This eventually leads to a crossover in the stiffness between two different scaling behaviors. When the solid volume fraction is far below that of the random dense limit of granular packings, the scaling of stiffness is 'membranic', and when the random dense packing is approached, the stiffness scaling becomes 'granular'. There is no obvious difference in the distribution of deformation energy in the two regimes. It thus seems that deformation ridges in membranes and force chains in granular packings are different manifestations of the same phenomenon.

-
- [1] Y. Kantor, M. Kardar, and D. Nelson, Phys. Rev. Lett. **57**, 791 (1986).
 - [2] A. Lobkovsky, S. Gentges, H. Li, D. Morse, and T.A. Witten, Science **270**, 1482 (1995).
 - [3] B.A. DiDonna and T.A. Witten, Phys. Rev. Lett. **87**, 206105 (2001).
 - [4] E. Cerda, S. Chaïeb, F. Melo, and L. Mahadevan, Nature **401**, 46 (1999).
 - [5] B.A. DiDonna, T.A. Witten, S.C. Venkataramani and E.M. Kramer, Phys. Rev. E **65**, 016603 (2002).
 - [6] P.A. Houle and J.P. Sethna, Phys. Rev. E **54**, 278 (1996).
 - [7] E. Helfer, S. Harlepp, L. Bourieu, J. Robert, F. C. MacKintosh, and D. Chatena, Phys. Rev. Lett. **87**, 088103 (2001).
 - [8] C. Liu, S.R. Nagel, D.A. Schecter, S.N. Coppersmith, S. Majumdar, O. Narayan, and T.A. Witten, Science **269**, 513 (1995).
 - [9] F. Radjai, M. Jean, J.-J. Moreau, and S. Roux, Phys. Rev. Lett. **77**, 274 (1996).
 - [10] E. Cerda and L. Mahadevan, Phys. Rev. Lett. **90**, 074302 (2003).
 - [11] K. Matan, R.B. Williams, T.A. Witten, and S.R. Nagel, Phys. Rev. Lett. **88**, 076101 (2002).
 - [12] H.A. Makse, D.L. Johnson, and L.M. Schwartz, Phys. Rev. Lett. **84**, 4160 (2000).
 - [13] B.A. DiDonna, Phys. Rev. E **66**, 016601 (2002).
 - [14] E.M. Kramer and T.A. Witten, Phys. Rev. Lett. **78**, 1303 (1997).
 - [15] A.E. Lobkovsky and T.A. Witten, Phys. Rev. E **55**, 1577 (1997).
 - [16] E. Cerda and L. Mahadevan, Phys. Rev. Lett. **80**, 2358 (1998).
 - [17] S. Chaïeb and F. Melo, Phys. Rev. E **60**, 6091 (1999).
 - [18] C.S. O'Hern, S.A. Langer, A.J. Liu, and S.R. Nagel, Phys. Rev. Lett. **88**, 075507 (2002).